Electron Spin Resonance and Electron Spin Echo Modulation Spectroscopy of Aluminophosphate-Based Mesoporous Molecular Sieve Containing Framework Manganese

Dongyuan Zhao, Zhaohua Luan, and Larry Kevan*

Department of Chemistry, University of Houston, Houston, Texas 77204-5641

Received: April 9, 1997; In Final Form: July 1, 1997[⊗]

Aluminophosphate-based mesoporous molecular sieves with variable amounts of framework manganese have been synthesized at room temperature using cationic surfactant cetyltrimethylammonium chloride as a structure-directing agent. Powder X-ray diffraction shows that all solid products with a *d* spacing of about 0.42 nm are structurally similar to silica-based MCM-41 materials. After calcination at 500 °C to decompose the surfactant these products still show a single broad diffraction peak with a *d* spacing of 0.36 nm and high surface area (830−930 m^2/g), indicating that the products are relatively thermally stable. Electron probe microanalysis shows that the incorporation of Mn^{2+} causes an increase of the framework P/Al ratio from about 0.6 for manganese-free samples to about 0.7 for manganese-containing samples; these values are lower than 1.0 for an ideal aluminophosphate framework. This increase in P/Al ratio may account for the improved thermal stability of aluminophosphate mesoporous molecular sieves upon incorporation of Mn^{2+}. Electron spin resonance and electron spin echo spectroscopy reveal that Mn^{2+} in both as-synthesized and calcined products is immobile and inaccessible to adsorbates such as water, ammonia, and pyridine. This suggests that Mn^{2+} is located in the mesoporous aluminophosphate framework. This is confirmed by ^{31}P electron spin echo modulation which shows that Mn^{2+} is associated with three phosphorus atoms at a distance of 0.34 nm.

Introduction

In 1992 researchers at Mobil Corp. synthesized the M41S family of silica-based mesoporous molecular sieves with pore sizes from 2.0 to 10 nm.[1] This stimulated interest to develop mesoporous aluminophosphate molecular sieves. Aluminophosphates (AlPO-*n*) are another well-known family of crystalline microporous materials.[2] VPI-5 is an aluminophosphate with the largest channels containing rings of 18 tetrahedral (T) atoms.[3] New aluminophosphate molecular sieves with large pores are in demand for potential use as catalysts for large molecule transformations.[4−9]

Several research groups have attempted to prepare aluminophosphate-based mesostructure materials. Oliver et al.[10] and Sayari et al.[11] have synthesized lamellar mesostructure aluminophosphate by using an amphiphilic alkylamine as a template in tetraethylene glycol solvent and in water, respectively. Unfortunately, these materials are thermally unstable. More recently, Kimura et al. have reported in a conference abstract that a hexagonal mesostructured aluminophosphate mixed with a lamellar phase was synthesized.[12] We have also successfully synthesized hexagonal mesoporous aluminophosphate and silicoaluminophosphate molecular sieves with ∼4.0 nm pore sizes which have reasonable thermal stability.[13]

It has been shown that incorporation of transition metal ions into microporous aluminophosphate successfully improves its Bronsted acidity and increases the potential of these materials as catalysts.[14−16] Here we report a successful synthesis of manganese-substituted aluminophosphate-based mesoporous molecular sieve with a hexagonal structure, reasonable thermal stability, and high specific surface area. The location of the Mn^{2+} ion is characterized by electron spin resonance (ESR) and electron spin echo modulation (ESEM) spectroscopy.

Experimental Section

Synthesis. Mesoporous aluminophosphate (UHM-1) was synthesized as described previously[13] by using cetyltrimethylammonium chloride (CTAC, Aldrich, 25 wt % in water) as the structure-directing agent and aluminum hydroxide (53.5 wt % of Al_2O_3, USP, Pfaltz & Bauer Inc.) and phosphoric acid (85 wt %, EM Industries) as the aluminum and phosphorus sources. In a typical preparation of the synthesis gel, 3.53 g of aluminum hydroxide was slowly added to a solution of 8.5 g of phosphoric acid in 25 g of water under vigorous stirring. The mixture was added to a solution of 11.6 g of cetyltrimethylammonium chloride in 100 g of water under stirring. After 3 h, 34 g of tetramethylammonium hydroxide (TMAOH, Aldrich, 25 wt % in water) was dropped into the above mixture until pH 9.0 was achieved.

Manganese-substituted mesoporous aluminophosphate (Mn-UHM-1) was synthesized by using a similar procedure, except that an amount of 0.2 M $MnCl_2$ (Aldrich) solution for the desired Mn/Al ratio was added into the aluminophosphate gel with stirring before the addition of the CTAC surfactant solution. The composition of the resultant gel was Al_2O_3:$x$$P_2O_5$:$y$MnO:$\mu$CTAC:$\nu$TMAOH:$\omega$$H_2O$, where $x = 0.6-3.37$, $y = 0-0.4$, $\mu = 0.24-0.50$, $\nu = 8.5-46.7$, and $\omega = 200-642$.

The gels obtained using these procedures were stirred for 72 h at room temperature to promote crystallization. The solid product was filtered, washed with deionized water and air-dried at 70 °C. The template was removed by calcination at 500 °C for 1 h in flowing nitrogen, followed by 6 h in flowing oxygen.[1]

For comparison, Mn^{2+} ion-exchanged into mesoporous aluminophosphate (Mn−UHM-1) was prepared as follows. A 5 mL quantity of 10^{-3} M $MnCl_2$ solution was added to 0.5 g of calcined UHM-1 aluminophosphate and 100 mL of deionized water; the mixture was stirred at room temperature for 24 h, filtered, washed thoroughly with hot deionized water, and then allowed to air-dry. This process is termed ion exchange because P/Al < 1; see below.

Characterization. Powder X-ray diffraction (XRD) patterns of the products were obtained on a Siemens D5000 diffractometer with a scan rate of 1 °C/min and Cu Kα radiation ($\lambda =$ 0.154 18 nm). Thermogravimetric analysis (TGA) was per-

[⊗] Abstract published in *Advance ACS Abstracts,* August 15, 1997.

S1089-5647(97)01217-0 CCC: $14.00

TABLE 1: Elemental Composition of the Gel Mixture and Solid Products of Manganese-Containing Mesoporous Aluminophosphate (MnUHM-1) Materials

gel mixture		solid product		BET surface area (m^2/g)
P/Al	Mn/Al	P/Al	Mn/Al	
2.0	0	0.64	0	790
2.0	3.0×10^{-4}	0.71	4.8×10^{-4}	930
2.0	0.01	0.72	1.6×10^{-2}	830
2.0	0.10	0.70	0.15	900
2.0	0.20	0.78	0.33	900

formed on a DuPont 2100 thermal analyzer with a heating rate of 10 °C/min in air. Surface areas of the samples were measured on a monosorb (Quantachrome Corp.) automated direct reading surface area analyzer by the single point method. Electron probe microanalysis was performed on a Jeol JXA-8600 spectrometer. Table 1 gives the elemental composition and surface areas of the resultant solid products.

ESR and ESEM Measurement. Samples were activated in 2 mm i.d. × 3 mm o.d. Suprasil quartz tubes that were attached to a vacuum line. Activation or dehydration of the sample was carried out by first evacuating the sample at room temperature. Then the temperature was raised slowly over an 8 h period to 250 °C and held at that temperature under a pressure of 1×10^{-5} Torr overnight. The samples were then cooled to room temperature under vacuum. D_2O (Aldrich), ND_3 (Stohler), and C_5D_5N (Linde) were purified of dissolved gases by freezing at 77 K, pumping to low pressure under vacuum, thawing to room temperature in a closed system, and repeating for typically three times until no residual pressure was detected at 77 K. These purified chemicals were then used as adsorbates. The activated samples were equilibrated with the saturated room-temperature vapor pressure of the liquids, while 400 Torr of ND_3 was used. After equilibration, the samples were frozen in liquid nitrogen and sealed.

ESR spectra were recorded on a Bruker ESP 380 spectrometer at both room temperature and 77 K. Several scans (5−10) per sample were averaged. ESEM spectra were recorded at 5 K on a Bruker ESP 380 pulsed spectrometer using an Oxford Instruments CF 935 flowing liquid helium cryostat. Three-pulse stimulated echoes were recorded with a $\pi/2$, $\pi/2$, $\pi/2$ pulse sequence in which the echo intensity is measured as a function of the time, T, between the second and third pulses. The value for τ, the time between the first and second pulses, was selected to minimize modulation from ^{27}Al nuclei contained in the molecular sieve lattice. Phase cycling was employed to correct for two pulse glitches that occur at $T = \tau$ and $T = 2\tau$.[17]

The ESEM spectra were simulated with a ratio analysis procedure that has been described in detail elsewhere.[18,19] The value for N, the number of nearest equivalent nuclei around the paramagnetic center, was constrained to be integral. In general, N can be determined uniquely, while the value for R, the distance from the paramagnetic center to the nuclei, is determined to ±0.01 nm.

Results

XRD Studies. The XRD pattern of as-synthesized mesoporous aluminophosphate UHM-1 is shown in Figure 1a. As-synthesized UHM-1 exhibits a XRD pattern of typical hexagonal mesoporous materials,[1,20] which show an intense diffraction peak near $2\theta \sim 2°$, which corresponds to a (100) reflection consistent with a repeat distance between pores of about 4.0 nm (Figure 1a). The weaker peaks correspond to (110), (200), and (210) reflections, consistent with a hexagonal lattice for the pores. These weaker peaks can be observed at higher gain, but compared to MCM-41 the (200) and (210) reflections are broader and not as well resolved, indicating a less ordered hexagonal mesoporous structure of this aluminophosphate material compared to MCM-41.

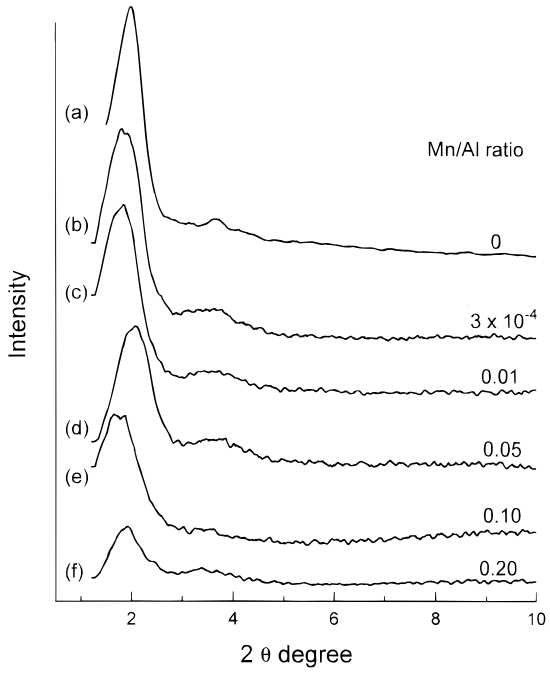

Figure 1. Powder XRD patterns of as-synthesized manganese-containing mesoporous aluminophosphate MnUHM-1 with variable Mn/Al gel ratio.

Electron probe microanalysis shows that UHM-1 has a unique composition over a solid particle, but the P/Al ratio is only about 0.64 (Table 1). This result indicates that the UHM-1 material has a nonideal aluminophosphate framework compared to microporous crystalline AlPO-n materials.

As-synthesized MnUHM-1 materials with a variable Mn/Al gel ratio (3×10^{-4}−0.20) also give similar XRD patterns (Figure 1b−f) with a (100) reflection corresponding to about 4.2 nm, similar to the case of UHM-1. With increasing manganese content the resolution of the XRD pattern of MnUHM-1 deteriorates in the $2\theta = 3°-4°$ region, especially when the Mn/Al ratio approaches 0.20 (Figure 1f). Figure 1d seems offset slightly to larger 2θ for unknown reasons. Also, the product becomes nonhomogeneous by electron microprobe data for a Mn/Al gel ratio larger than 0.20. Attempts to synthesize a pure manganophosphate mesostructure failed.

Electron probe microanalysis shows that manganese in the products synthesized with a Mn/Al gel ratio less than 0.20 is rather homogeneously distributed over a solid particle, and the Mn/Al ratio is comparable with that in the initial gel mixture (Table 1). We also note that the P/Al ratio in MnUHM-1 products is about 0.70, which is less than the ideal value of 1.0 and less than the initial gel mixture, but slightly higher than that of UHM-1. MnUHM-1 still has a nonideal aluminophosphate framework, but incorporation of manganese seems to increase the P/Al ratio.

The XRD pattern (Figure 2a) of calcined UHM-1 exhibits only a single diffraction peak corresponding to a d spacing of 3.6 nm. The other weak (110), (200), and (210) reflections are broadened beyond detection. The broadening of higher order reflections is usually acknowledged to arise from a lack of long-range crystallographic order.[21,22] We also note that the intensity of the d (100) reflection of calcined UHM-1 decreases in comparison with that of as-synthesized UHM-1. The results indicate that the UHM-1 materials become more disordered after

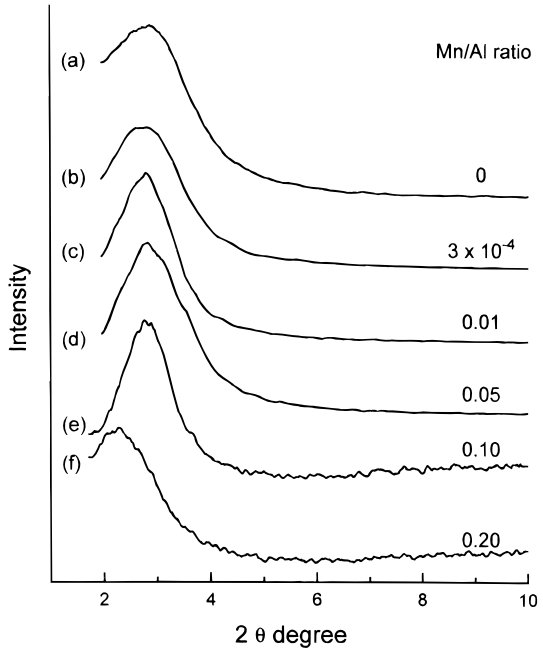

Figure 2. Powder XRD patterns of calcined (500 °C) manganese-containing mesoporous aluminophosphate MnUHM-1 with variable Mn/Al gel ratio.

calcination. Transmission electron microscopy also shows that calcined UHM-1 is more disordered than as-synthesized UHM-1.

All calcined MnUHM-1 materials also exhibit a (100) peak corresponding to a *d* spacing of ∼3.6 nm (Figure 2b−e), except MnUHM-1 with a Mn/Al gel ratio of 0.20 (Figure 2f). This diffraction peak is narrower than for UHM-1, especially for a Mn/Al gel ratio of 0.10, which suggests that incorporation of manganese can improve the thermal stability. We also note that MnUHM-1 with a Mn/Al gel ratio of 0.20 shows a weak diffraction reflection corresponding to 4.0 nm, indicating structural deterioration. All MnUHM-1 materials show slightly higher BET surface areas (830−930 m^2/g) than UHM-1 (790 m^2/g) which are independent of the Mn/Al ratio (Table 1).

TGA Studies. Thermogravimetric analysis of UHM-1 shows a large weight loss of ∼70% on heating to 700 °C. Three endothermic losses near 80 °C (15% weight loss), 240 °C (30% weight loss), and 340 °C (25% weight loss) are observed. The 80 °C weight loss is assigned to water desorption. The 240 and 340 °C weight losses are assigned to desorption and decomposition of TMAOH and CTAC in either order. Mn-UHM-1 shows a similar TGA curve as UHM-1, but the total weight loss of ∼55% is less than ∼70% for UHM-1. The lower weight loss for MnUHM-1 appears to indicate less total organic template incorporated.

ESR Studies. As-synthesized MnUHM-1 with a Mn/Al gel ratio of 3×10^{-4} exhibits a typical Mn^{2+} ESR spectrum with a six-line hyperfine coupling of ∼82 G and $g = 2.008$ (Figure 3), which corresponds to a $m_s|\ -\ ^1/_2\rangle \rightarrow |+^1/_2\rangle$ transition.[23−27] The other transitions are not resolved due to their large anisotropies; they contribute mostly to the background upon which the six narrower lines are superimposed. The small peaks in between the six major hyperfine lines represent forbidden transitions involving $\Delta m_1 = \pm 1$ and indicating that the zero-field splitting is nonnegligible.[25,26] As-synthesized MnUHM-1 exhibits these forbidden transitions at both room temperature and 77 K, consistent with an immobile Mn^{2+} species.[23,28]

All as-synthesized MnUHM-1 with higher Mn/Al ratio (0.01−0.1) give similar ESR parameters of $g = 2.008$ and $A =$ ∼82 G but with less resolved hyperfine lines (spectra not shown). As-synthesized MnUHM-1 with the highest Mn/Al ratio of 0.2 loses all hyperfine resolution and only exhibits a single broad line ($\Delta H_{pp} \sim 530$ G).

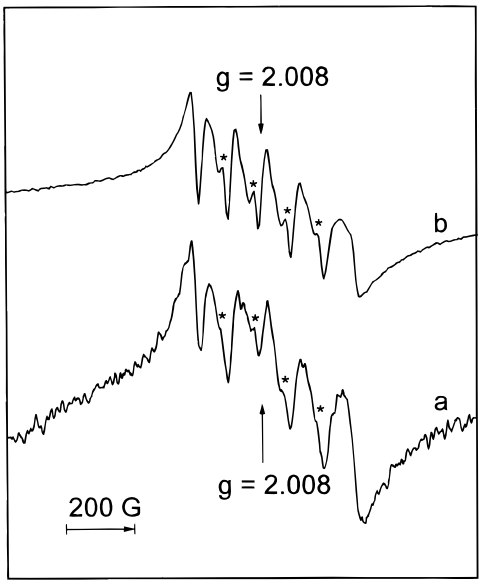

Figure 3. X-band ESR spectra of as-synthesized MnUHM-1 with Mn/Al gel ratio of 3×10^{-4} at (a) room temperature and (b) 77 K. The asterisks indicate forbidden transitions. Both spectra are averages of 10 scans.

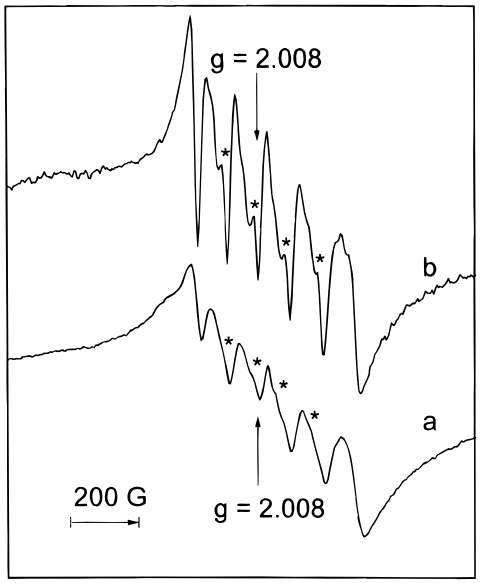

Figure 4. X-band ESR spectra of calcined MnUHM-1 with Mn/Al gel ratio of 3×10^{-4} at (a) room temperature and (b) 77 K. The asterisks indicate forbidden transitions. Spectrum a is an average of 10 scans, and spectrum b is an average of five scans.

After calcination at 500 °C, MnUHM-1 with a Mn/Al ratio of 3×10^{-4} exhibits an ESR spectrum similar to the as-synthesized form (Figure 4), but the hyperfine coupling seems shifted somewhat from 82 to 86 G. Forbidden transitions are observed at both room temperature and 77 K, consistent with an immobile Mn^{2+} species.[23,28] All other calcined MnUHM-1 with higher Mn/Al ratios (0.01−0.1) show similar ESR parameters of $g = 2.008$ and $A = 85 \sim 86$ G, but with poorly resolved hyperfine lines. Calcined MnUHM-1 with the highest Mn/Al ratio of 0.2 exhibits only a single broad line like its as-synthesized form.

A broad line without hyperfine splitting at $g = 4.30$ is observed for all as-synthesized and calcined MnUHM-1 samples,

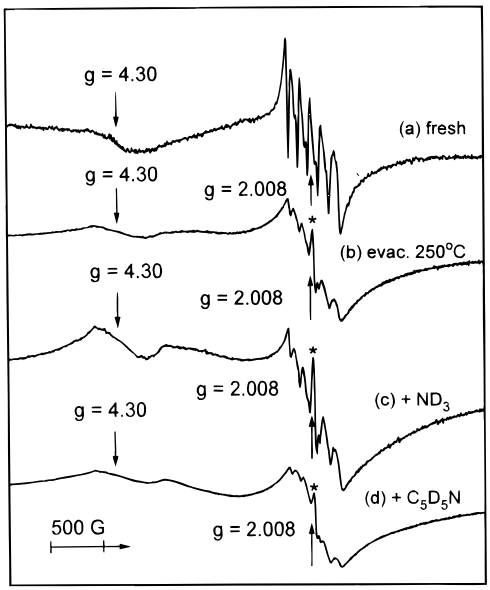

Figure 5. X-band ESR spectra at 77 K of synthetic mesoporous MnUHM-1 materials: (a) fresh, calcined, (b) after evacuation at 250 °C overnight, (c) after adsorption of ammonia (ND_3), and (d) after adsorption of pyridine (C_5D_5N). The asterisk indicates an unknown paramagnetic center.

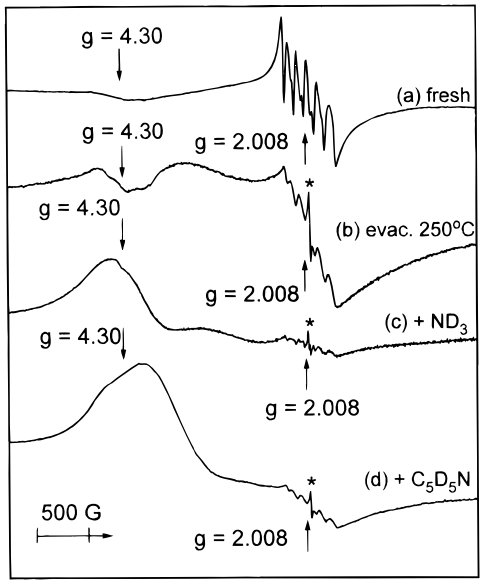

Figure 6. X-band ESR spectra at 77 K of Mn^{2+} ion-exchanged into mesoporous aluminophosphate material denoted Mn−UHM-1: (a) fresh, (b) after evacuation at 250 °C overnight, (c) after adsorption of ammonia (ND_3), and (d) after adsorption of pyridine (C_5D_5N). The asterisk indicates an unknown paramagnetic center.

as shown in Figure 5a for calcined MnUHM-1 with a Mn/Al ratio of 3×10^4. The line width of this line is about 530 G, which is similar to that of the line at $g = 2.008$. This low field resonance will be discussed below.

After dehydration by evacuation at 250 °C overnight, MnUHM-1 (Figure 5b) shows an ESR spectrum similar to its fresh calcined form (Figure 5a), but with poorer hyperfine resolution and a slightly increased hyperfine coupling from 82 to 85 G. After adsorption of ammonia (ND_3), the ESR spectrum (Figure 5c) remains similar to the dehydrated sample (Figure 5b), but the relative intensity of the peak at $g = 4.30$ is increased. A similar result is observed for adsorbed pyridine (C_5D_5N), except that the peak at $g = 4.30$ is almost unchanged (Figure 5d). The ESR spectra of MnUHM-1 in Figure 5b−d also show an additional sharp line at $g \approx 2$, denoted by an asterisk, which is assigned to an unknown paramagnetic center formed during calcination and evacuation.

For comparison, the ESR spectra of Mn^{2+} ion-exchanged into UHM-1 (Mn−UHM-1) and after dehydration and adsorption of ammonia and pyridine are shown in Figure 6. Fresh Mn−UHM-1 shows an ESR spectrum similar to that of MnUHM-1 at $g = 2.008$, but the hyperfine coupling is larger (89 G) than for MnUHM-1 and the forbidden transitions at room temperature are a little weaker than in MnUHM-1, indicating some mobility of the Mn^{2+} species. After evacuation at 250 °C overnight, the peak at $g = 4.30$ increases much more than for MnUHM-1. After adsorption of ND_3 or C_5D_5N on Mn−UHM-1, the $g = 4.30$ peak increases substantially. Also, the ESR sextet at $g = 2.008$ becomes quite weak. These differences from MnUHM-1 indicate that the Mn^{2+} species in Mn−UHM-1 is more accessible to adsorbates.

ESEM Studies. In order to obtain more quantitative information about the location of the Mn^{2+} species in Mn-UHM-1 materials, three-pulse ESEM spectra of at 5 K of MnUHM-1 and Mn−UHM-1 materials were compared. Echo-detected field swept spectra at 5 K give absorption spectra rather than derivative spectra and are poorly resolved, but do show the same overall spectra as at 77 K so that the relaxation times are still short enough to make valid comparisons with 77 K data. Figure 7 shows a three-pulse ESEM spectrum of dehydrated MnUHM-1 with evacuation at 250 °C overnight. The spectrum was recorded at an external magnetic field of 3480 G, corresponding approximately to the $g = 2.0$ position, where the echo intensity reaches a maximum, and τ was 0.248 μs to eliminate modulation from ^{27}Al nuclei and maximize modulation from ^{31}P nuclei. MnUHM-1 shows relatively strong modulation from ^{31}P nuclei ($I = {}^1/_2$), which is simulated for $N = 3$ ^{31}P at distance $R = 0.34$ nm with isotropic hyperfine coupling $A_{iso} = 0.20$ MHz. The fit is not as good as typical, which may indicate overlapping Mn^{2+} species.

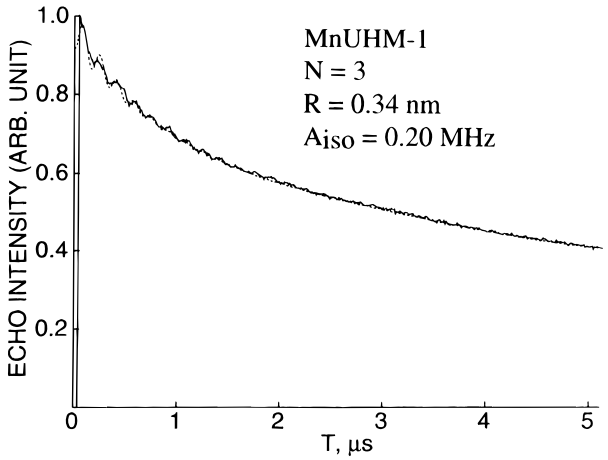

Figure 7. Experimental (—) and simulated (- - -) three-pulse ESEM spectra at 5 K of mesoporous MnUHM-1 material after calcination at 500 °C in air and evacuation at 250 °C overnight. The first interpulse time τ of 0.248 μs was selected to maximize the modulation depth from ^{31}P and eliminate the modulation from ^{27}Al.

Figure 8 shows three-pulse deuterium ESEM spectra of MnUHM-1 with adsorbed D_2O. The deuterium modulation is quite weak. The best fit to the experimental spectrum is $N = 2$ at $R = 0.40$ nm with $A_{iso} = 0.06$ MHz, which corresponds to one indirectly coordinated water molecule. However, Mn−UHM-1 after adsorption of D_2O shows much stronger deuterium modulation (Figure 9) than MnUHM-1. The simulation for Mn−UHM-1 of $N = 6$ at 0.31 nm indicates that Mn^{2+} is coordinated to three water molecules at a direct coordination

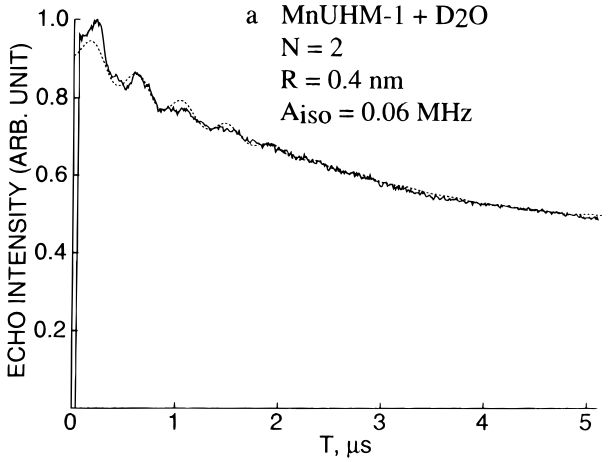

Figure 8. Experimental (—) and simulated (- - -) three-pulse ESEM spectra at 5 K of calcined and evacuated MnUHM-1 material with adsorbed water (D_2O).

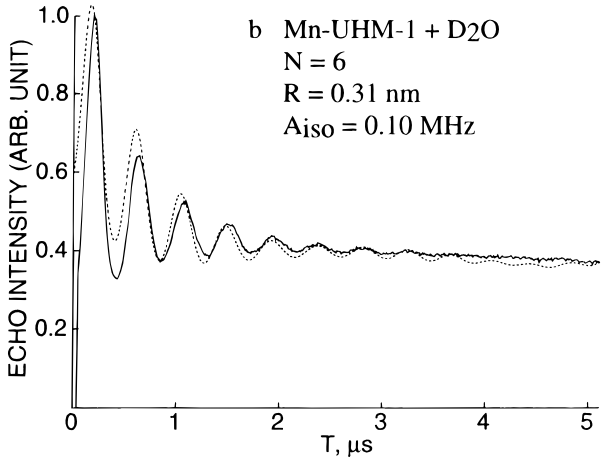

Figure 9. Experimental (—) and simulated (- - -) three-pulse ESEM spectra at 5 K of Mn^{2+} ion-exchanged into mesoporous aluminophosphate material (Mn−UHM-1) material with adsorbed water (D_2O).

distance of 0.31 nm. Although these spectral fits are again not as good as expected, the data clearly indicate a distinct difference in the local water coordination to MnUHM-1 versus Mn−UHM-1, which is the important conclusion.

No attempt was made to fit the strong aluminum modulation because of the additional parameters needed for the large quadrupole interaction. Typically, ^{27}Al modulation has not been too useful in determining local environmental structure in powder samples.

Discussion

Aluminophosphate-based hexagonal mesoporous materials have been successfully synthesized in basic medium in the presence of tetramethylammonium hydroxide (TMAOH) by using cationic cetyltrimethylammonium chloride as the structure-directing agent.[13] We postulate that the formation of aluminophosphate-based hexagonal mesoporous materials occurs by a modified S^+I^- ion pair process, which is consistent with the so-called liquid-crystal "templating" mechanism[1b] and electrostatic complementary assembly between the inorganic species and the charged surfactant headgroup.[20] The inorganic precursor (I^-) is an aluminophosphate-based species of low polymerization degree. Some hydroxyl groups of these aluminophosphate-based species react with TMAOH to produce a very weak ion pair ($I^-\cdots TMA^+$) since the TMA cation has a large ionic radius. This weak ion pair diffuses to the surfactant assembly (S^+) interface, and the (I^-) part interacts with the cationic surfactant headgroup. Continuous condensation of adjacent inorganic species occurs to form an ordered hexagonal mesostructure. The aluminophosphate-based mesoporous materials can be synthesized with a variable P/Al ratio, and elemental analysis shows that the P/Al ratio of the product is less than 1.0. This suggests that excess hydroxyl aluminum species are involved in the assembly on the micelle interface to form the mesoporous material. The nonideal composition of the materials may cause the lower thermal stability aluminophosphate-based mesoporous materials compared to silica-based MCM-41 materials.

Incorporation of manganese into the framework of aluminophosphate-based mesoporous materials is shown to be successful in this work. The incorporation of manganese seems to improve the thermal stability compared to UHM-1 materials. This may be due to the higher P/Al ratio observed for MnUHM-1. This reasoning is only based on the observation that AlPO-*n* with P/Al = 1 shows higher thermal stability.

Evidence for immobile Mn^{2+} located in the framework of mesoporous aluminophosphate is shown by ESR and ESEM spectra. Two possible locations for Mn^{2+} in the as-synthesized product are in the inorganic wall or at the interface region of the polar headgroup of the surfactant. However, in the second location Mn^{2+} should have some mobility and so is probably excluded. ESEM spectra indicate that Mn^{2+} is associated with three phosphorus nuclei, which is consistent with a framework location.

After calcination, the ESR spectra (Figure 4) at room temperature show forbidden transitions consistent with an immobile Mn^{2+} species. This is quite different from previous reports with manganese in silica-based mesoporous materials,[23] in which Mn^{2+} showed an environment similar to a solution and is mobile. Also, the interaction of Mn^{2+} in MnUHM-1 with ammonia and pyridine adsorbates differs from that for ion-exchanged Mn−UHM-1 (Figure 6). It is striking that the $g = 4.30$ peak associated with Mn^{2+} varies so much in intensity with adsorbates and between MnUHM-1 (Figure 5) and Mn−UHM-1 (Figure 6). The interpretation of this $g = 4.30$ peak is somewhat controversial[29−34] although it can be ascribed to transitions in the $M_s = \pm 3/2$ doublet for a high-spin $S = 3/2$ system in a rhombic ligand field.[33,34] The intensity changes may be related to the degree of rhombic distortion of the Mn^{2+} environment, but we have been unable to relate this to any specific local structural model thus far. Nevertheless, the $g = 4.30$ results appear to indicate significant differences between the local environment of Mn^{2+} in MnUHM-1 versus Mn−UHM-1, especially in the presence of ammonia and pyridine adsorbates. The overall results indicate that Mn^{2+} in synthesized MnUHM-1 is inaccessible to adsorbates and that Mn^{2+} in ion-exchanged Mn−UHM-1 is accessible to adsorbates. These results clearly indicate that Mn^{2+} in MnUHM-1 is located in a different site than Mn^{2+} in Mn−UHM-1.

The ESEM results further confirm that the Mn^{2+} species is located in the framework of MnUHM-1. Figure 7 shows that Mn^{2+} in MnUHM-1 is associated with three phosphorus atoms at 0.34 nm, which is consistent with Mn^{2+} replacing an aluminum atom in the nonideal mesoporous framework (see Table 1). Thus, Mn is tetrahedrally bonded to four oxygens, which are bonded to four phosphorus atoms in the MnUHM-1 framework. Additional interaction or coordination to adsorbates also occurs. Figure 8 for MnUHM-1 with adsorbed D_2O shows weak deuterium modulation from two deuterium atoms interacting at 0.40 nm. This distance is too long for direct coordination to D_2O but is consistent with Mn^{2+} being in the framework of MnUHM-1 and interacting weakly with one or two adsorbed

waters on the large channel wall. This is all the water adsorbates that are expected to be accessible to Mn^{2+} located in the mesoporous material framework. In striking contrast, Mn^{2+} in Mn−UHM-1 is directly coordinated to six deuteriums, which is interpreted as three molecules of water at 0.31 nm, corresponding to an $Mn^{2+}-O(D_2O)$ distance of ∼0.24 nm which is close to a direct coordination distance. Mn^{2+} in ion-exchanged Mn−UHM-1 is likely located in the large channel weakly coordinated to framework oxygens. It is then accessible for direct coordination with adsorbate water.

Conclusions

Aluminophosphate-based mesoporous molecular sieves UHM-1 and MnUHM-1 have been successfully synthesized. The latter contains a variable amount of framework manganese, which is confirmed by electron spin resonance and electron spin echo modulation spectroscopy. MnUHM-1 shows high specific surface area (790−930 m^2/g) and is relatively thermally stable after calcination at 500 °C to decompose the surfactant. The framework of UHM-1 and MnUHM-1 contains a nonideal P/Al ratio less than 1.0. ESR and ESEM results reveal that Mn^{2+} in both as-synthesized and calcined MnUHM-1 is immobile, relatively inaccessible to adsorbates such as water, ammonia, and pyridine, and located in the framework of mesoporous aluminophosphate interacting with three phosphorus atoms. In contrast, Mn^{2+} in ion-exchanged Mn−UHM-1 is in a totally different site and is directly coordinated to three water molecules.

Acknowledgment. This research was supported by the National Science Foundation, the Robert A. Welch Foundation, and the University of Houston Energy Laboratory.

References and Notes

(1) (a) Kresge, C. T.; Leonowicz, M. E.; Roth, W. J.; Vartuli, J. C.; Beck, J. S. *Nature* **1992**, *359*, 710. (b) Beck, J. S.; Vartuli, J. C.; Roth, W. J.; Leonowicz, M. E.; Kresge, C. T.; Schmitt, K. D.; Chu, C. T.-W.; Olson, D. H.; Sheppard, E. W.; McCullen, S. B.; Higgins, J. B.; Schlenker, J. L. *J. Am. Chem. Soc.* **1992**, *114*, 10834.

(2) Wilson, S. T.; Lok, B. M.; Messina, C. A.; Connan, T. R.; Flanigan, E. M. *J. Am. Chem. Soc.* **1982**, *104*, 1146.

(3) Davis, M. E.; Saldamaga, C.; Montes, C.; Garces, J.; Crowder, C. *Nature* **1988**, *331*, 698.

(4) Davis, M. E. *Chem. Ind.* **1992**, *4*, 137.

(5) Estemann, M.; McCusker, L. B.; Baerlocher, C.; Merroche, A.; Kessler, H. *Nature* **1991**, *352*, 320.

(6) Davis M. E. *Nature* **1991**, *352*, 281.

(7) Davis, M. E. *Nature* **1989**, *337*, 117.

(8) Smith, J. V.; Dytrych, W. J. *Nature* **1984**, *309*, 607.

(9) Brunner, G. O.; Meier, W. M. *Nature* **1989**, *337*, 147.

(10) Oliver, S.; Kuperman, A.; Coombs, N.; Louth, A.; Ozin, G. A. *Nature* **1995**, *378*, 47.

(11) (a) Sayari, A.; Karra, V. R.; Reddy, J. S.; Moudrakovski, I. L. *J. Chem. Soc., Chem. Commun.* **1996**, 411. (b) Chenite, A.; Page, Y. L.; Karra, V. R.; Sayari, A. *J. Chem. Soc., Chem. Commun.* **1996**, 413. (c) Sayari, A.; Moudrakovski, I. L.; Reddy, J. S. *Chem. Mater.* **1996**, *8*, 2080. (d) Sayari, A. In *Progress in Zeolite Microporous Materials;* Chon, H., Ihm, S.-K., Uh, Y. S., Eds.; Studies in Surface and Catalysis, Vol. 105; Elsevier: Amsterdam, 1997; pp 37−44.

(12) Kimura, T.; Sugahara, Y.; Kuroda, K. *11th International Zeolite Conference Abstract* RP45; Seoul, Korea, 1996.

(13) Zhao, D.; Luan, Z.; Kevan, L. *J. Chem. Soc., Chem. Commun.* **1997,** 1009.

(14) Iton, L. E.; Choi, I.; Desjardins, J. A.; Maroni, V. A. *Zeolites* **1989**, *9*, 457.

(15) Shiralkar, V. P.; Saldariaga, C. H.; Perez, J. O.; Clearfield, A.; Chen, M.; Anthony, R. G.; Donohue, J. A. *Zeolites* **1989**, *9*, 474.

(16) Schoonheydt, R. A.; de Vos, R.; Pelgrims, J.; Leeman, H. In *Zeolites: Facts, Figures and Future;* Jacobs, P. A.; van Santen, R. A., Eds.; Elsevier: Amsterdam, 1989; p 559.

(17) Fauth, J. M.; Schweiger, A.; Brauschweiler, L.; Forrer, J.; Ernst, R. R. *J. Magn. Reson.* **1986**, *66*, 74.

(18) Kevan, L. In *Time Domain Electron Spin Resonance;* Kevan, L., Schwartz, R. N., Eds.; Wiley-Interscience: New York, 1979; Chapter 8.

(19) Kevan, L.; Bowman, M. K.; Narayana, P. A.; Boeckman, R. K.; Yudanov, V. F.; Tsvetkov, Yu. D. *J. Chem. Phys.* **1975**, *63*, 409.

(20) (a) Huo, Q.; Margolese, D. I.; Cielsa, U.; Feng, P.; Gier, T. E.; Sieger, P.; Leon, R.; Petroff, P. M.; Schuth, F.; Stucky, G. D. *Nature* **1994**, *368*, 317. (b) Huo, Q.; Margolese, D. I.; Cielsa, U.; Demuth, D. G.; Feng, P.; Gier, T. E.; Firouzi, A.; Chmelka, B. F.; Schuth, F.; Stucky, G. D. *Chem. Mater.* **1994**, *6*, 1176.

(21) (a) Tanev, P. T.; Pinnavaia, T. J. *Science* **1995**, *267*, 865. (b) Bagshaw, S. A.; Prouzet, E.; Pinnavaia, T. J. *Science* **1995**, *269*, 1242. (c) Tanev, P. T.; Chibwe, M.; Pinnaviaia, T. J. *Nature* **1994**, *368*, 321.

(22) Chen, C.-Y.; Li, H.-Y.; Burkett, S. L.; Davis, M. E. *Microporous Mater.* **1993**, *2*, 27.

(23) (a) Zhao, D.; Goldfarb, D. *J. Chem. Soc., Chem. Commun.* **1995**, 875. (b) Zhao, D.; Goldfarb, D. In *Zeolites: a Refined Tool for Designing Catalytic Sites*; Bonneviot, L., Kaliaguine, S., Eds.; Studies in Surface and Catalysis, Vol. 97; Elsevier: Amsterdam, 1995; p 181.

(24) Levi, Z.; Raitsimring, A. M.; Goldfarb, D. *J. Phys. Chem.* **1991**, *95*, 7830.

(25) Olender Z.; Goldfarb, D.; Batista, J. *J. Am. Chem. Soc.* **1993**, *115*, 1106.

(26) Brouet, G.; Chen, X.; Lee, C. W.; Kevan, L. *J. Am. Chem. Soc.* **1992**, *114*, 3720.

(27) Lee, C. W.; Chen, X.; Brouet, G.; Kevan, L. *J. Phys. Chem.* **1992**, *96*, 3110.

(28) Meirovitch, E.; Poupko, R. *J. Phys. Chem.* **1978**, *82*, 1920.

(29) (a) Purans, J.; Kliava, J.; Millere, I. *Phys. Status Solidi A* **1979**, *56*, K25. (b) Kliava, J. G.; Purans, J. J. *Phys. Status Solidi A* **1978**, *49*, K43.

(30) Zhilinskaya, E. A.; Lazukin, V. N.; Bychkov, E. A.; Rosenkov, S. B. *Phys. Status Solidi B* **1988**, *149*, 427.

(31) Karge, H. G. In *Progress in Zeolites and Microporous Materials;* Chon, H., Ihm, S.-K., Uh, Y. S., Eds.; Studies in Surface Science and Catalysis, Vol. 105; Elsevier: Amsterdam, 1997; p 1901.

(32) Wichterlova, B.; Beran, S.; Bednarova, S.; Nedomov, K.; Dudikova, L.; Jiru, P. In *Innovation in Zeolite Materials Science*; Grobet, P. J., Mortier, W. J., Vasant, E. F., Schulz-Ekloff, G., Eds.; Studies in Surface Science and Catalysis, Vol. 37; Elsevier: Amsterdam, 1988; p 199.

(33) Kliava, J. *Phys. Status Solidi B* **1986,** *134*, 411.

(34) Pilbrow, J. R. *Transition Ion Electron Paramagnetic Resonance;* Oxford Press: Oxford, 1990; pp 306−308, 135−138.